AIAA JOURNAL
Vol. 32, No. 2, February 1994

Reactive and Viscous Flow in Hypersonic Nozzles

D. Zeitoun,* E. Boccaccio,† M. C. Druguet,† and M. Imbert‡
Université de Provence—St. Jérôme, Marseille, France

In high-enthalpy hypersonic facilities, the airflow at the exit of a convergent-divergent nozzle is affected by the high reservoir enthalpy level because chemical and vibrational nonequilibrium processes take place in the nozzle. The models in the test section are generally located at the nozzle exit, and so the knowledge of the nozzle flowfield is of upmost importance to obtain the upstream conditions for the flow around the model. This flowfield is studied numerically by solving the unsteady laminar axisymmetric Navier-Stokes equations, coupled with those describing the chemical and thermal nonequilibrium processes in the real-air gas mixture. The equations are solved by an implicit time-dependent finite difference method, including a flux-splitting technique in the implicit operator. Results show the flowfield in conical and contoured nozzles for different high-enthalpy reservoir conditions. The chemical and vibrational nonequilibrium behavior in the boundary layer and in the core flow is also emphasized.

Introduction

A BETTER knowledge of chemical and thermodynamical nonequilibrium processes related to aerodynamic aspects is needed to study the re-entry phase of the Space Shuttle. Within this research area, many numerical approaches, taking into account more or less complicated nonequilibrium models, have been developed.[1-4] To validate these computations, several hypersonic facilities have been built, such as, for example, the free-piston shock tunnel (TCM2) at the Université de Provence in Marseille,[5] within the framework of the European Hermes program. In such a facility, hypersonic flow is obtained at the exit of a convergent-divergent nozzle, under high-enthalpy reservoir conditions, produced in a free-piston shock tube. The test section is located at the nozzle exit, and to know the nominal flow properties, it is necessary to compute the flowfield in the nozzle before the experiments, for two reasons. First, contrary to real flight, the flow around the model is spatially nonuniform, due to the shape of the divergent part of the nozzle and to boundary-layer effects. Second, the thermodynamic and chemical states of the flow are typically in nonequilibrium, due to the freezing resulting from the rapid expansion in the nozzle. Thus, accurate prediction of the upstream flowfield is essential.

The flow regimes in a convergent-divergent nozzle transition sequentially from subsonic, transonic and supersonic, to hypersonic. At the same time, energy exchanges take place, which give rise to physico-chemical processes, like the vibrational excitation of diatomic molecules, dissociation, and ionization. Successively, equilibrium, nonequilibrium, and frozen zones are present, depending on the local ratio between the characteristic relaxation time of each process and the flow time.[6] The flow parameters depend on the concentration of each gas mixture component and on the vibrational energy distribution of diatomic molecules. The continuous interaction of the chemical and thermodynamical processes with the flow is taken into account by the coupling between the equations that describe these processes.

Received Nov. 5, 1992; revision received June 15, 1993; accepted for publication July 16, 1993.

*Professor of Fluid Dynamics, Lab. I.U.S.T.I. (U.R.A. CNRS 1168) Departement Milieux Hors d'Equilibre, 13397 Marseille Cedex 20. Member AIAA.

†Graduate Student, Lab. I.U.S.T.I. (U.R.A. CNRS 1168) Departement Milieux Hors d'Equilibre, 13397 Marseille Cedex 20.

‡Maître de Conférence, Lab. I.U.S.T.I. (U.R.A. CNRS 1168) Departement Milieux Hors d'Equilibre, 13397 Marseille Cedex 20.

The present work consists of a modeling and a numerical simulation of a reactive viscous hypersonic flow in an axisymmetric wind-tunnel nozzle. In high-enthalpy reservoir conditions, the air is dissociated and may be considered as a mixture of the five species—N_2, O_2, NO, N, and O—in an equilibrium state. In the axisymmetric nozzle, the hypersonic airflow is in a chemical and thermal nonequilibrium state. The diatomic molecule NO is taken to be in thermal equilibrium, because its vibrational relaxation time is found experimentally to be orders of magnitude smaller than those in N_2 and O_2.[7] The chemical kinetics are based on a 17-reaction model, with the corresponding rate constants given by Park.[8] The source terms in the vibrational energy equations include the vibration-translation and vibration-vibration exchanges and the coupled-vibration-dissociation-vibration (CVDV) model. This last formulation also modifies the forward rate constants of the chemical kinetics.[9]

The system of equations considered is the Navier-Stokes equations with the five mass conservation equations for the chemical species and the two vibrational energy conservation equations for N_2 and O_2. This system of 10 equations is solved by a noniterative implicit finite difference scheme, with a flux-splitting technique in the implicit operator.[10-11] This method was chosen to overcome two principal difficulties. The first one is the stiffness of the problem, due to the chemical and vibrational processes, and the second one is the need for using fine meshes near the wall to capture correctly the boundary-layer effects. After discretization, the linear system is a block-pentadiagonal matrix and can be solved by either the Gauss-Seidel line or point relaxation methods. This implicit approach also allows the use of a larger integration time step than that imposed by the Courant-Friedrichs-Lewy (CFL) condition, and this reduces the CPU time required to reach steady state.

Two nozzle shapes have been considered. The first is conical with 45 and 10 deg convergent-divergent angles and an exit area ratio of 4444 over a 1.12-m length. This nozzle has been chosen as the 8.2 test case of Ref. 12, with pressure and temperature reservoir conditions taken as $P_0 = 1530$ bars and $T_0 = 6500$ K, respectively. A value of $P_0 = 1000$ bars was also tested. The second configuration is a contoured nozzle with an exit area ratio of 4480 over a 3.40-m length and reservoir conditions of $P_0 = 2000$ bars and $T_0 = 8500$ K. Results show the evolution of the flow parameters in the boundary layer and the core flow and the chemical and vibrational nonequilibrium and freezing behavior along the nozzles. A comparison with Gnoffo's computations[13] is also made for the 8.2 test case.

Governing Equations

In a cylindrical coordinate system, the axisymmetric conservation equations for an air mixture in a thermal and chemical nonequilibrium state can be expressed in vector form as

$$\partial_t U + \partial_x(F_e + F_v) + \partial_y(G_e + G_v) + \frac{1}{y}H_a + H_s = 0 \qquad (1)$$

The vector of conservative quantities is given by

$$U = [\rho_s(s = 1, \ldots, 5), \rho u, \rho v, \rho E, \rho_i e_{v_i}(i = 1, 2)]^T \qquad (2)$$

where ρ_s is the density of each species; the subscript s represents the five species—N, O, NO, N_2, and O_2—of the air mixture; $i = 1, 2$ refers to the diatomic species N_2 and O_2 (NO is assumed to be in a thermal equilibrium state); ρ is the density of the mixture; u and v are the components of the velocity V; and ρE is the total energy per unit volume, containing translational, rotational, and vibrational energies, the latent chemical energy of the species, and the kinetic energy of directed motion; ρE is given by

$$\rho E = \sum_{s=1}^{5} \rho_s c_{v_s} T + \sum_{i=1}^{2} \rho_i e_{v_i} + \rho_{NO} e_{v_{NO}} + \sum_{s=1}^{5} \rho_s h_s^{for} + \tfrac{1}{2}\rho V^2 \qquad (3)$$

In Eq. (1), the vectors F_e and G_e represent the Eulerian convective fluxes, whereas the viscous terms F_v and G_v contain the transport term expressions, such as diffusion velocity of each species, stress tensor, and heat flux. In these expressions, the viscosity and the thermal conductivity of the mixture are calculated from Wilke's mixing rule,[14] and the binary diffusion coefficient from the empirical formula given by Chapman and Cowling.[15] The vector H_a includes the axisymmetric terms of the equations. A detailed description of these vectors can be found in Ref. 16. The vector $H_s = (\omega_s, 0, 0, 0, \omega_i)^T$ contains the chemical source terms ω_s, due to the net rate production of each species, and the vibrational source terms ω_i of the species N_2 and O_2. These source terms are the result of the chemical and vibrational nonequilibrium modeling and are described hereafter.

Chemical Nonequilibrium Modeling

In the air mixture, each species is considered as a perfect gas. The chemical source terms are derived from the reactions that occur between these species. They are given by the following 17-reaction scheme[8]:

$$\begin{aligned} N_2 + M &\rightleftharpoons 2N + M \\ O_2 + M &\rightleftharpoons 2O + M \\ NO + M &\rightleftharpoons N + O + M \\ N_2 + O &\rightleftharpoons NO + N \\ NO + O &\rightleftharpoons N + O_2 \end{aligned} \qquad (4)$$

with $M =$ N, O, NO, N_2, and O_2.

The magnitude of mass production or removal is obtained from

$$\omega_s = M_s \sum_r (\nu''_{sr} - \nu'_{sr}) \left[k_{f_r} \prod_s \left(\frac{\rho_s}{M_s}\right)^{\nu'_{sr}} - k_{b_r} \prod_s \left(\frac{\rho_s}{M_s}\right)^{\nu''_{sr}} \right] \qquad (5)$$

where ν'_{sr} and ν''_{sr} refer to the stoichiometric coefficients, whereas the forward and backward reaction rates k_f and k_b are given by the Arrhenius rate equations. These equations are computed using the translational temperature with coefficients given by Park.[8] If one takes into account the coupling between chemical and vibrational processes, the forward reaction rate k_f of the dissociation equations is modified as follows:

$$k_f^c = k_f V \qquad (6)$$

where V represents the coupling factor, which depends on the vibrational modeling, through the ratio of partition functions Q[9]:

$$V = \frac{Q(T)}{Q(T_{V_i})} \frac{Q(T_{F_i})}{Q(-U_i)} \qquad (7)$$

where T is the translational-rotational temperature, T_{V_i} is the vibrational temperature deduced from the vibrational energy of the diatomic species i, and T_{F_i} is an average temperature defined by the following expression:

$$\frac{1}{T_{F_i}} = \frac{1}{T_{V_i}} - \frac{1}{T} - \frac{1}{U_i} \qquad (8)$$

where $(-U_i)$ can be considered as a temperature corresponding to the probability of dissociation from a vibrational level; its value depends on the model being considered. In the case of a nonpreferential model, the probability of dissociation is the same whatever the vibrational level, and $U_i = \infty$. But with the preferential model, the diatomic molecules dissociate preferentially from the upper levels, and the value of U_i is of the order of magnitude of the dissociation characteristic temperature θ_{D_i} (Ref. 9).

Vibrational Nonequilibrium Modeling

The coupling between chemical and vibrational processes also modifies the source terms ω_i in the vibrational equations of the diatomic species, which can be written as the sum of the different exchanges:

$$\omega_i = \omega_{i(T-V)} + \omega_{i(V-V)} + \omega_{i(C-V)} \qquad (9)$$

In this expression $\omega_{i(T-V)}$ represents the internal energy exchanges between the translational and vibrational modes and is classically described by the Landau-Teller formulation:

$$\omega_{i(T-V)} = \frac{\rho_i e_{V_i}^0 - \rho_i e_{V_i}}{\tau_i^{VT}} + e_{V_i}\omega_{s=1} \qquad (10)$$

where $e_{V_i}^0$ is the vibrational energy at equilibrium; since $\omega_{i(T-V)}$ takes into account all of the vibrational-translational exchanges, the global relaxation time τ_i^{VT} is expressed as:

$$\frac{1}{\tau_i^{VT}} = \sum_{s=1}^{5} \frac{\xi_s}{\tau_{is}^{VT}} \qquad (11)$$

where ξ_s is the molar fraction of each species s, and τ_{is}^{VT} is the relaxation time for the exchanges between the diatomic molecules i and any species s; τ_{is}^{VT} has the following general form:

$$p\tau_{is}^{VT} = a_{is} T^{b_{is}} \exp(-c_{is} T^{-1/3} + d_{is}) \qquad (12)$$

where a_{is}, b_{is}, c_{is}, and d_{is} are constants depending on the colliding species (which can be found in Ref. 16), and p is the pressure.

The $\omega_{i(V-V)}$ refers to the exchanges between the vibrational-vibrational modes of diatomic species:

$$\omega_{i(V-V)} = \frac{1}{\tau_{iJ}^{VV}} \frac{1}{\rho R \theta_{V_j}} \Big[\rho_j e_{V_j} (\rho_i e_{V_i} + \rho_i R_i \theta_{V_i}) \exp\left(\frac{\theta_{V_j} - \theta_{V_i}}{T}\right) - \rho_i e_{V_i} (\rho_j e_{V_j} + \rho_j R_j \theta_{V_j}) \Big] \qquad (13)$$

where R_i is the molar gas constant, θ_{V_i} is the vibrational characteristic temperature, and τ_{iJ}^{VV} is the relaxation time for $V - V$ exchanges.[17]

The last term, $\omega_{i(C-V)}$, corresponds to the dissociation-vibration coupling and arises due to the fact that the average vibrational energy of the molecule is partly determined by the chemical relaxation: a recombination or a dissociation of a molecule leads to a gain or a loss in the average vibrational energy:

$$\omega_{i(C-V)} = -[\overline{e_{V_i}}(T_{F_i}) - e_{V_i}(T_{V_i})] \left[\frac{d(\rho_i)}{dt}\right]_f + [\overline{e_{V_i}}(-U_i) - e_{V_i}(T_{V_i})] \left[\frac{d(\rho_i)}{dt}\right]_b \qquad (14)$$

where $\overline{e_{V_i}}(T_{F_i})$ is the average value of the vibrational energy lost in one dissociation and $\overline{e_{V_i}}(-U_i)$ is that gained with each recombination. Under equilibrium conditions, $\overline{e_{V_i}}(-U_i)$ is the limit of $\overline{e_{V_i}}(T_{F_i})$ when T_{V_i} tends to T; $\overline{e_{V_i}}(T_{F_i})$ can be written as[9]

$$\overline{e_{V_i}}(T_{F_i}) = \frac{R_i\theta_{V_i}}{\exp(\theta_{V_i}/T_{F_i})-1} - \frac{N_iR_i\theta_{V_i}}{\exp(N_i\theta_{V_i}/T_{F_i})-1} \tag{15}$$

where N_i is the number of vibrational levels corresponding to the dissociation energy of the molecule i.

It is important to note that the influence of each term in this vibrational nonequilibrium model will be computed in an inviscid nozzle flow. This will eventually allow simplification of the model when treating the viscous case.

Computational Procedure

The unsteady flow equations (1) must be integrated in time from an initial solution for the convergent-divergent axisymmetric hypersonic nozzle with given reservoir and wall conditions. The complete physico-chemical model is used with an assumption of inviscid flow to evaluate the influence of the various processes on the flow parameters and to deduce some simplifications. Then viscous effects are analyzed to obtain more realistic predictions of properties along the axis and at the exit section of the nozzle.

To correctly describe the dissipative effects in the wall boundary layer that develops along the nozzle and the strong flow gradients around the nozzle throat, the mesh distribution must be quite stretched, and consequently the explicit integration time step is very small. To overcome this difficulty and others, due to the stiffness of the chemical and vibrational equations, the system of 10 governing equations (1) is solved by a strongly implicit finite difference scheme like that used by MacCormack.[10] The physical domain (x, y) is transformed into a rectangular one (ξ, η), and for each node (i, j) of this domain the system of equations is written at each time step $(n+1)\Delta t$ as

$$\frac{U^{n+1}-U^n}{\Delta t} + \frac{D}{D\xi}(F_e+F_v)^{n+1} + \frac{D}{D\eta}(G_e+G_v)^{n+1} + \frac{1}{y}H_a^{n+1} + H_s^{n+1} = 0 \tag{16}$$

If Φ represents one of the vectors of this equation, it is linearized to yield the expansion

$$\Phi^{n+1} = \Phi^n + \left(\frac{\partial\Phi}{\partial U}\right)^n \delta U^n \tag{17}$$

where $(\partial\Phi/\partial U)$ is the Jacobian matrix and $\delta U^n = U^{n+1} - U^n$.

Under these conditions, and after having split the vectors F_e and G_e into a positive and a negative part with the nondissipative flux-splitting technique,[18] the system (16) is equivalent to

$$\left[I + \Delta t\left(\frac{D_+A_-}{\Delta\xi} + \frac{D_-A_+}{\Delta\xi} + \frac{D^2S_v}{\Delta\xi^2} + \frac{D_+B_-}{\Delta\eta} + \frac{D_-B_+}{\Delta\eta} + \frac{D^2R_v}{\Delta\eta^2} + \frac{1}{y}C_a + C_s\right)\right]\delta U^n = \Delta U^n \tag{18}$$

In this equation, D, D_+, and D_- are, respectively, central, forward, and backward difference operators, whereas A_-, A_+, S_v, B_-, B_+, R_v, C_a, and C_s are the Jacobian matrices of F_e^-, F_e^+, F_v, G_e^-, G_e^+, G_v, H_a, and H_s; C_a contains only the Jacobian of the nondissipative part of the vector H_a.

After discretization, the system (18) may be written as a pentadiagonal matrix linear system:

$$\hat{B}_{i,j}\delta U^n_{i,j+1} + \hat{A}_{i,j}\delta U^n_{i,j} + \hat{C}_{i,j}\delta U^n_{i,j-1} + \hat{D}_{i,j}\delta U^n_{i+1,j} + \hat{E}_{i,j}\delta U^n_{i-1,j} = \Delta U^n_{i,j} \tag{19}$$

At each time step, a predictor-corrector scheme is used, and the system (19) is solved by a Gauss-Seidel line or point relaxation method, with alternating sweeps in the backward and forward ξ direction. The conservation vector U is updated by

$$U^{n+1}_{i,j} = U^n_{i,j} + \delta U^n_{i,j} \tag{20}$$

The knowledge of the vector U allows us to obtain the following variables: ρ_s $(s = 1, \ldots, 5)$, ρ, u, v, e_{V_i} $(i = 1, 2)$. After that, the temperature is deduced from Eq. (3) using a Newton-Raphson iteration, and the pressure is found through the state equation of the gas mixture.

Boundary conditions of the computational domain are the following:

1) At the wall nozzle, the translational and vibrational temperatures are given, $u = v = 0$, $\partial P/\partial n = 0$, and the wall is assumed to be fully catalytic.

2) At the symmetry axis, the reflecting image principle is used.

3) At the exit boundary, all flow variables are extrapolated from the computed values.

4) For the inlet boundary, a detailed description is given in a previous paper.[11]

During the iterative procedure leading to the steady state, the integration step time Δt was increased from 5 to 1×10^3 Δt_{CFL}.

Conditions of Numerical Simulation

As mentioned earlier, two nozzles have been studied: a conical and a contoured one.

For the conical nozzle, the main dimensions, such as convergent and divergent angles α and β, throat and exit radii r^* and r_e, and total and divergent length L and l, are reported in Table 1. The reservoir conditions of pressure, temperature, speed of sound, and species concentrations, which are obtained by an equilibrium assumption, and wall conditions are also given in Table 1. These reservoir conditions correspond to a reduced total enthalpy H_0/RT^0 ($RT^0 = 288 \times 273$ J/Kg) equal to 131. In this nozzle, a lower value of the reservoir pressure of 1000 bars was also tested to study the influence of the reservoir pressure in the practical operating range of the facility; for this case the reservoir conditions are also recorded in Table 1.

A grid resolution study was performed to determine the number of points required in the ξ and η directions to capture correctly the flow gradients around the throat region and in the boundary layer.[16] In the first application, a mesh system of 64×72 points is used with $\Delta x_{\min} = 3.24 \times 10^{-4}$ m located at the throat section, and $\Delta y_{\min} = 2.1\ 10^{-8}$ m at the wall, with 51 mesh points in the boundary layer. In the lower pressure case, the mesh distribution was of 64×81 points. A steady-state solution for the nonequilibrium flow in the whole nozzle was obtained in 7000 iterations, with an integration step time that increased from 5 to 1×10^3 Δt_{CFL}.

Table 1 Geometrical dimensions and reservoir conditions of the nozzles

	α, deg	β, deg	r^*, m	r_e, m	L, m	l, m
	45	10	$3\ 10^{-3}$	0.20	1.13	1.12
	P_0, bars	T_0, K	a_0, m/s	Y_{N_2}	Y_{O_2}	Y_{NO}
Reservoir conditions for conical nozzle: case I	1530	6500	1710	0.689	0.0535	0.156
Reservoir conditions for conical nozzle: case II	1000	6500	1725	0.693	0.0455	0.144
Reservoir conditions for contoured nozzle: case III	2000	8500	2057	0.674	0.0143	0.112
Wall conditions	$T_w = 600$ K		Fully catalytic wall			

In hypersonic facilities, contoured nozzles are often used to obtain uniform hypersonic flow at the nozzle exit. The shape of this kind of nozzle leads generally to a length of the divergent part of several meters. In the present numerical simulation, a contoured nozzle has been chosen of 3.41-m length with an exit section ratio of 4480 and a throat diameter of 1 cm, like the previous conical nozzle. The reservoir conditions are also given in Table 1, and wall conditions are the same as those given in Table 1. In this example, the reduced total enthalpy (H_0/RT^0) was equal to 200. The mesh system was of 125×72 points, and the steady state was obtained after about 10,000 iterations.

In these nozzle computations, it was noticed that a steady state was obtained after about 700 iterations in the convergent section and around the throat region.

The numerical simulations were performed on a Cray II computer, and the CPU time/pt/iteration was equal to 2×10^{-3}s using the line Gauss-Seidel relaxation. This CPU time was reduced by a factor of 2 by using a point Gauss-Seidel relaxation.

Discussion of Results

The inviscid nozzle flow was first studied numerically. Previous results[18] have shown that the vibration-vibration exchanges and the vibration-chemical coupling processes have very little effect on the evolution of the flow parameters. The maximum effect is on the $T_{V_{O_2}}$ evolution and is on the order of

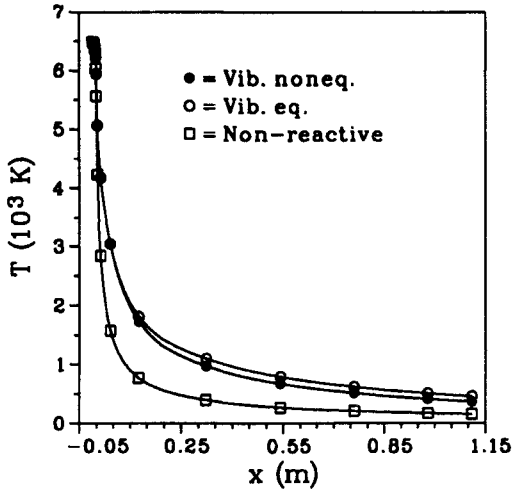

Fig. 1 Centerline temperature distributions for the three different assumptions.

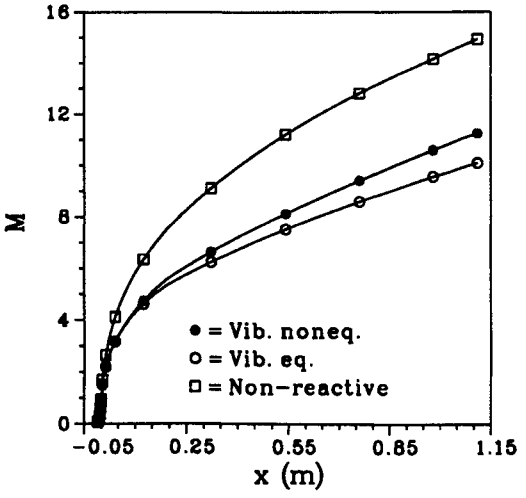

Fig. 2 Centerline Mach number distributions for the three different assumptions.

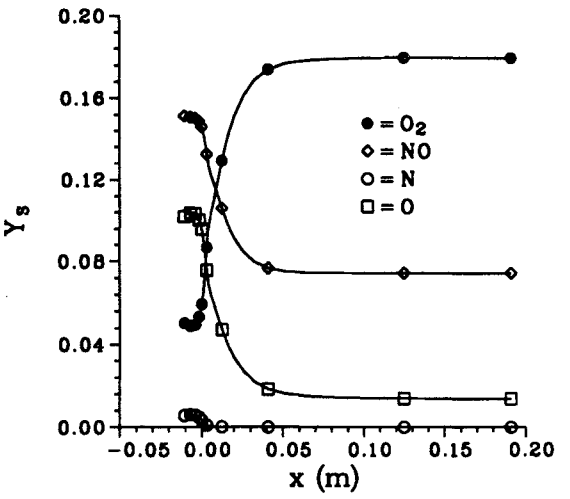

Fig. 3 Centerline species mass fraction distributions for the three different assumptions.

about 5%. On the basis of these results, the very fast freezing of the nonequilibrium effects and the decrease of translational temperature along the nozzle, these two processes have been neglected in the numerical model; therefore, only the translational-vibrational exchanges are taken into account in the vibrational modeling. It is obvious that these conclusions are only valid for this kind of nozzle for the specified reservoir conditions.

Conical Nozzle

Influence of Nonequilibrium Processes

For the first case, three computations were made to emphasize the importance of the nonequilibrium effects: 1) in chemical and vibrational nonequilibrium, 2) in chemical nonequilibrium supposing vibrational equilibrium, and 3) a nonreactive gas flow computation. These three computations are, respectively, called "Vib noneq," "vibeq," and "non-reactive" in Figs. 1 and 2. These figures show, respectively, the axial evolution (throat located at $x = 0$ cm) of the translational-rotational temperature T and the Mach number. They reveal the existence of a wide discrepancy between the nonreactive computation and the nonequilibrium one, pointing to the importance of the nonequilibrium processes on the flow properties. A variation of about 30% in the axial Mach number at the nozzle exit section was predicted. In fact, exothermic chemical reactions lead to an increase of the temperature of the gas mixture and so to a reduction in Mach number. However, the misfit in temperature between the two nonequilibrium cases is less important. This difference in behavior can be explained by the freezing of the vibrational energy levels, resulting in a decrease of the temperature T. Because the vibration-chemical coupling has been neglected, the influence of vibrational nonequilibrium on the evolutions of species mass fractions is negligible; therefore, only the axial evolution of mass fractions for the full nonequilibrium case is shown in Fig. 3. Equilibrium, nonequilibrium, and frozen zones can be observed. The flowfield is chemically frozen at 7 cm, where the dissociation of NO and the recombination of O_2 can be noted. At the center of the exit section, the mixture is composed of 74% N_2, 18% O_2, 7% NO, and 1% O.

Code-to-Code Comparison

As experimental results are not yet available, a comparison with Gnoffo's numerical results,[13] obtained with 40×80 mesh points, is made. Figure 4 shows the predicted centerline evolution of the temperature: good agreement between computed results for the two computations was obtained in the throat region where the gradients are important. A discrepancy is apparent after the first 30 cm of nozzle length. From this

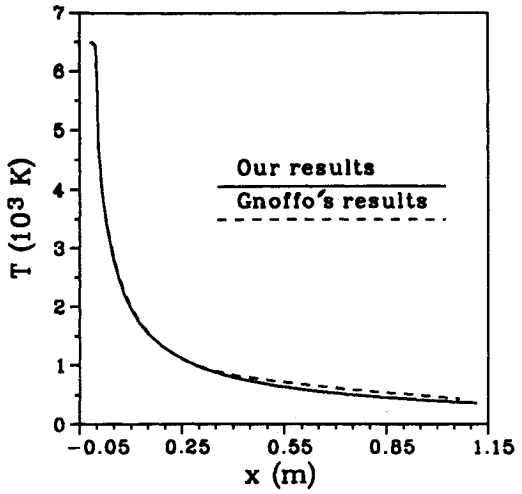

Fig. 4 Comparison of centerline temperature distributions.

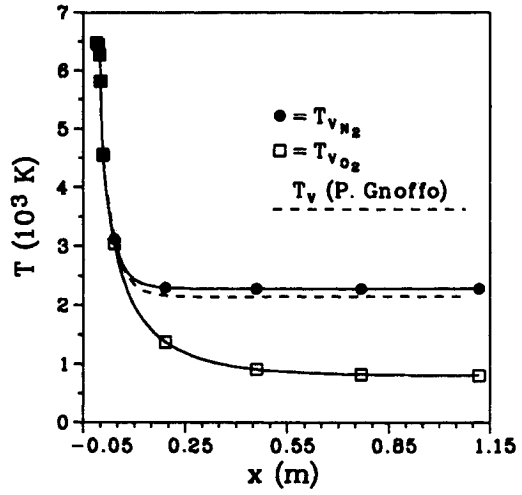

Fig. 5 Comparison of centerline vibrational temperature distributions.

section downstream, the freezing vibrational energy of the diatomic species O_2 becomes in the nozzle, as shown in Fig. 5, where the centerline evolution of vibrational temperatures is plotted. The discrepancy was a result of the two different vibration models adopted. In the present work, a three-temperature model was used, whereas Gnoffo used only two temperatures.

The influence of these different models is less important on the evolution of species mass fractions. For example, Fig. 6 represents the centerline evolution of O_2; the discrepancy is about 3% between the two simulations. But in Gnoffo's calculations the exit Mach number, equal to 10, is lower by about 10% than that obtained in the present calculations ($M = 11.2$).

Figures 7 and 8 show a comparison of the transverse profiles of temperature and velocity in a section at $x = 1.07$ m near the nozzle exit. These profiles are shown for only 10% of the nozzle exit radius, which corresponds to the boundary-layer thickness. Notice that the same value of the core flow velocity is predicted and that the velocity profiles have a slightly different shape (Fig. 7). Considering the temperature profiles, the discrepancy in the maximum values is about 150 K, and moreover the peaks are not located at the same distance from the nozzle wall (Fig. 8). These discrepancies can be explained, first, by the vibrational modeling that modifies the translational temperature, as deduced from Eq. (3), and, second, by the different expressions of the transport coefficients, and, finally, by the choice of flux-vector splitting.

Influence of the Stagnation Pressure

A stagnation pressure of 1530 bars may be impractical in the Marseille facility. For this reason a computation with 1000 bars was made to study the influence of the stagnation pres-

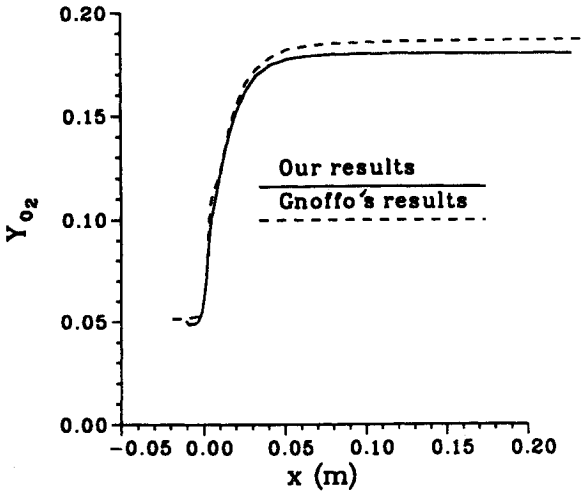

Fig. 6 Comparison of centerline mass fraction distributions of O_2.

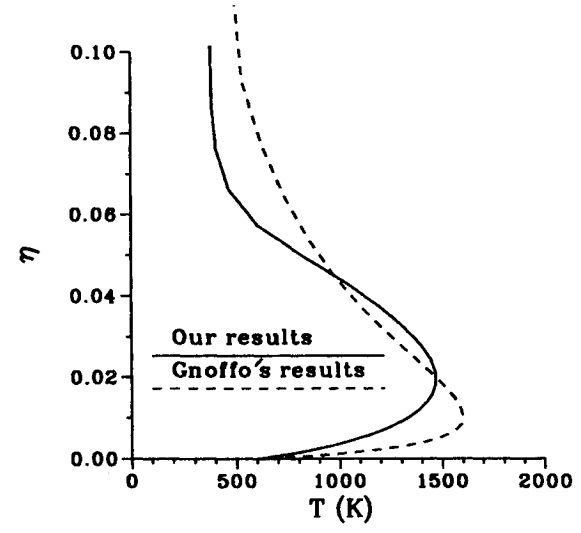

Fig. 7 Comparison of temperature transverse profiles in the boundary layer at $x = 1.07$ m.

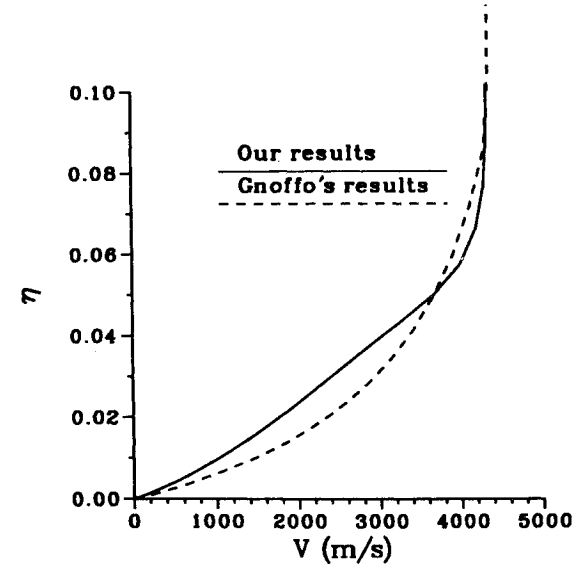

Fig. 8 Comparison of velocity transverse profiles in the boundary layer at $x = 1.07$ m.

sure on the flowfield parameters. The reservoir conditions corresponding to this pressure are indicated in Table 1. A comparison of the centerline evolution of the temperature and Mach number is shown in Figs. 9 and 10; a weak influence of the reservoir pressure is noted. At the exit section, a variation of about 1% can be observed in the Mach number and 2% on the vibrational temperature of N_2. However, although the level of freezing of Y_{N_2} was not influenced by the reduction of the stagnation pressure (Fig. 11), the freezing values of Y_{O_2} and Y_O were different for the two cases (Fig. 12). Therefore, it can be concluded that even though the flow parameters are weakly influenced by the stagnation pressure in the range of 1000–1530 bars, the air mixture composition depends on the pressure level. The two computational results are also compared using contour plots of Mach number (Fig. 13). The development of the boundary layer along the nozzle wall is

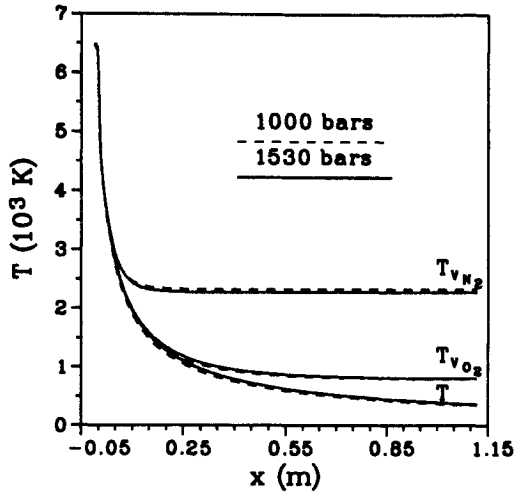

Fig. 9 Centerline temperature distributions at different reservoir pressures.

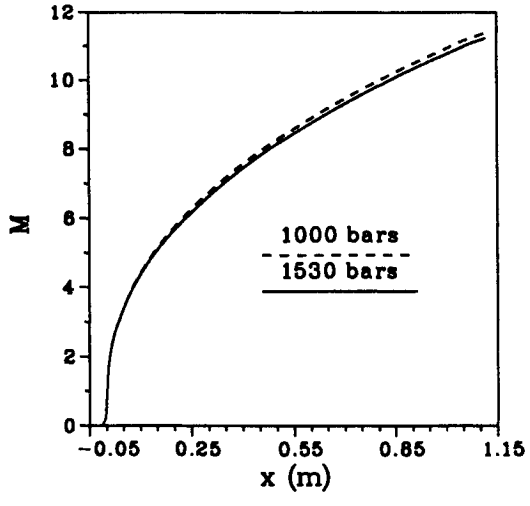

Fig. 10 Centerline Mach number distributions at different reservoir pressures.

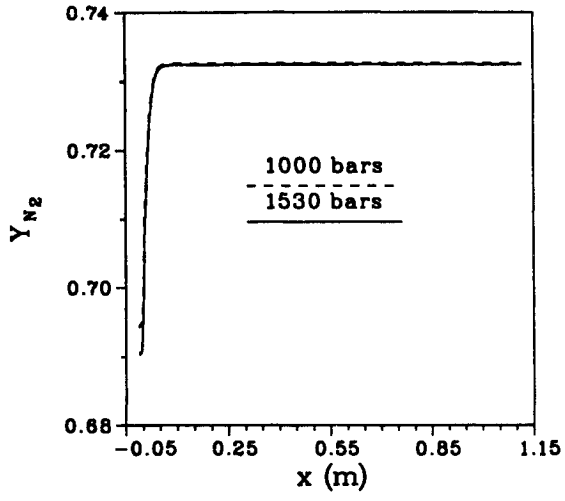

Fig. 11 Centerline N_2 mass fraction distribution at different reservoir pressures.

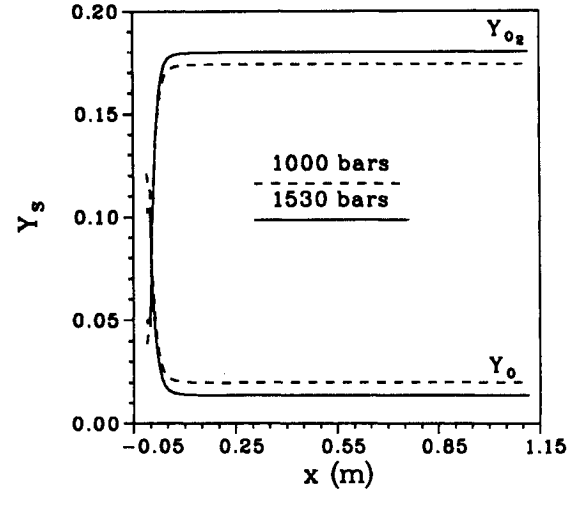

Fig. 12 Centerline species mass fraction distributions at different reservoir pressures.

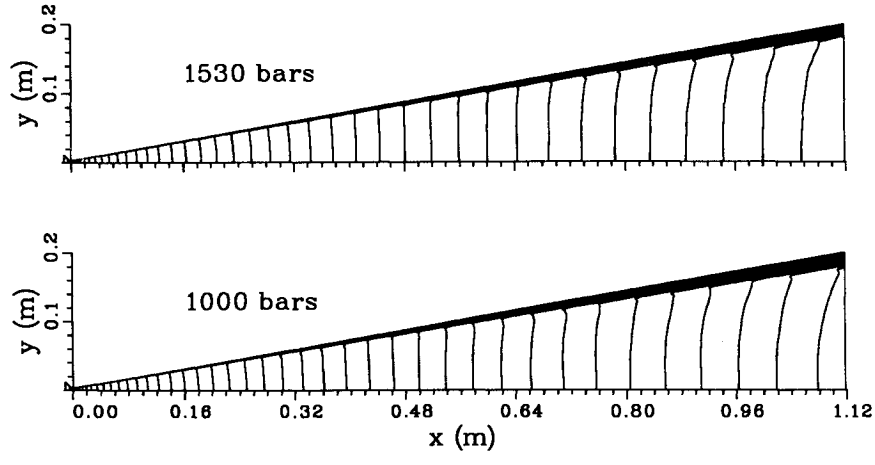

Fig. 13 Mach number contours ($\Delta M = 0.25$) at different reservoir pressures.

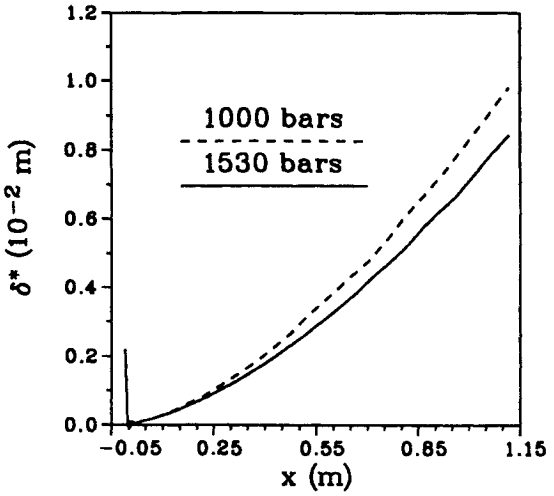

Fig. 14 Boundary-layer displacement thickness at different reservoir pressures.

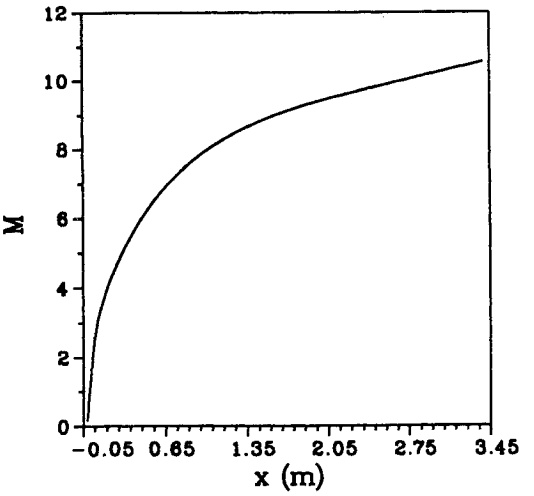

Fig. 16 Centerline Mach number distribution in the contoured nozzle.

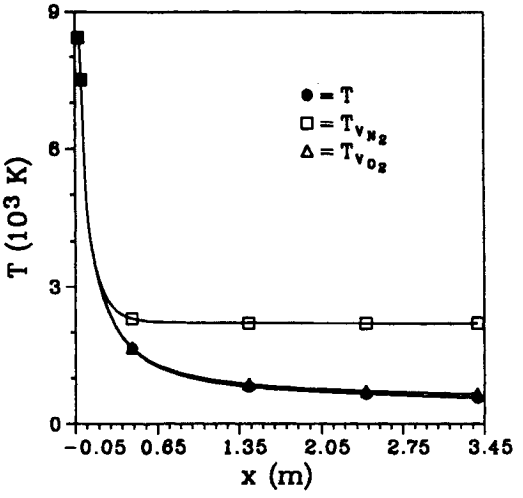

Fig. 15 Centerline temperature distributions in the contoured nozzle.

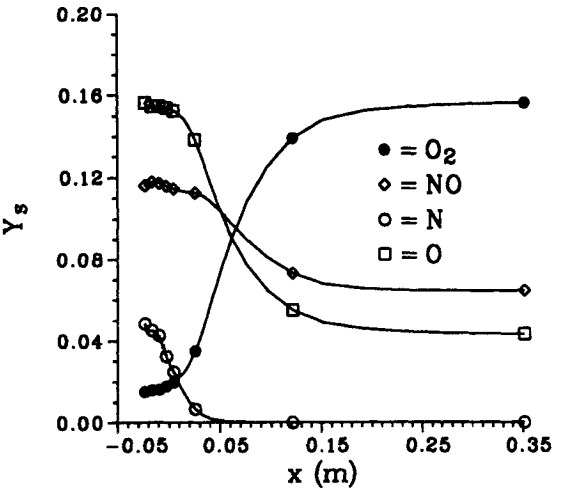

Fig. 17 Centerline species mass fraction distributions in the contoured nozzle.

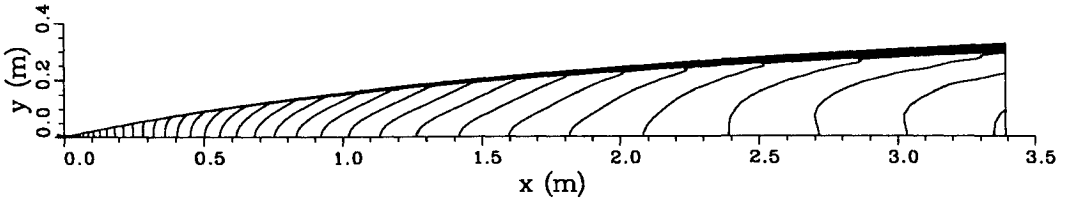

Fig. 18 Mach number contours ($\Delta M = 0.25$) in the contoured nozzle.

shown, and the boundary-layer thickness is about 10% of the exit radius; outside the boundary layer a uniform flowfield in the nozzle exit section can be observed. Finally, the boundary-layer displacement thickness δ^*, defined by the following expression,

$$R^2(x) - [R(x) - \delta^*(x)]^2 = 2\int_{R(x)-\delta(x)}^{R(x)} \left(1 - \frac{\rho u}{\rho_e u_e}\right) y \, dy \qquad (21)$$

is plotted on Fig. 14 for the two computations. A decrease of P_0 by 33% leads to an increase in δ^* of 18% at the nozzle exit section.

Contoured Nozzle Results

Numerical results of the computation of hypersonic flow for the contoured nozzle are now presented. The centerline evolutions of the various temperatures are plotted in Fig. 15. A freezing of $T_{V_{N_2}}$ is observed at 70 cm at a value about 2200 K, whereas $T_{V_{O_2}}$ is practically in vibrational equilibrium. The value of the translational-rotational temperature T at the exit plane is equal to 568 K. Figure 16 shows the centerline distribution of the Mach number M. A rapid increase of M was predicted for the first half of the divergent section and a linear progression for the second half, whereas the exit value of the Mach number is about 10.5. The centerline evolution of mass fractions is shown in Fig. 17. It shows that the flowfield is chemically frozen at 25 cm for Y_{NO} and at 31 cm for Y_{O_2} and Y_O. Contrary to results for the conical nozzle, the chemical and vibrational nonequilibrium regions are more important for this type of nozzle due to the higher value of the throat radius and the shape of the divergent section. Moreover, for the assumed nozzle contour, its shape does not lead to a

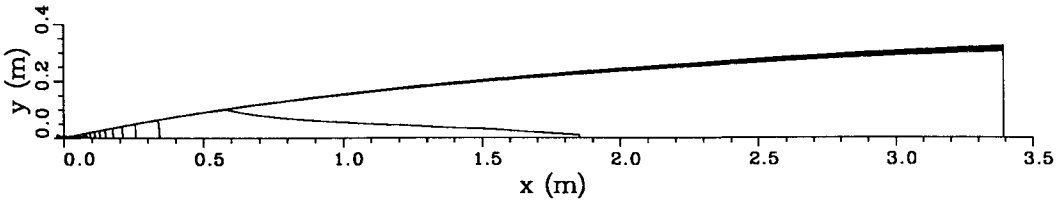

Fig. 19 N_2 vibrational temperature contours ($\Delta T_V = 200$) in the contoured nozzle.

uniform exit Mach number. The Mach and $T_{V_{N_2}}$ contours (Figs. 18 and 19) show a different behavior of the flowfield than in the conical nozzle. In each cross section, the flow is spatially nonuniform, due to a compression wave that appears at 30 cm from the curvature of the wall. At the nozzle exit section, a nonuniformity in the Mach number of about 0.5 was obtained (Fig. 18), and the freezing of $T_{V_{N_2}}$ in the divergent part of the nozzle followed this compression wave (Fig. 19).

Conclusions

Numerical simulations of hypersonic flows in conical and contoured nozzles have been carried out by solving the Navier-Stokes equations, taking into account the thermal and chemical nonequilibrium processes that occur in the air mixture flowfield.

A complete description of the flowfield in these nozzles has been obtained, and, more specifically, a knowledge was gained of the exit flow properties and the thermal and chemical behavior of the different species that make up the air mixture.

The numerical results show the influence of the pressure and the shape of the divergent part of the nozzle on the chemical and vibrational freezing levels and the growth of the boundary layer up to the exit section. They also show that it is easier to obtain an exit uniform flow with a conical nozzle than with a contoured nozzle; it is important to note that these exit properties will have to be used as initial flow conditions in flowfield studies of models in hypersonic facilities. A comparison with Gnoffo's results illustrates the influence of the vibrational model on the temperature distributions in the nozzle.

Acknowledgments

The authors would like to thank the Centre de Calcul Vectoriel de la Recherche for allowing access to the Cray II; this work is partially supported through the Hermes European Program.

References

[1]Candler, G., and MacCormack, R. W., "The Computational of Hypersonic Ionized Flows in Thermal and Chemical Nonequilibrium," AIAA Paper 88-0511, Jan. 1988.

[2]Gnoffo, P., "Upwind-Biased, Point-Implicit Relaxation Strategies for Viscous, Hypersonic Flows," AIAA Paper 89-1972-CP, June 1989.

[3]Boccaccio, E., Zeitoun, D., and Imbert, M., "Navier-Stokes Computation for Nonequilibrium Hypersonic Flows," *Computing Methods in Applied Sciences and Engineering*, edited by R. Glowinski, Nova Science Publishers, New York, 1992, pp. 321-330.

[4]Jusuyala, E., and Shang, J. S., "Computation of Hypersonic Flowfield in Thermal and Chemical Nonequilibrium," AIAA Paper 92-2874, July 1992.

[5]Burstchell, Y., Brun, R., and Zeitoun, D., "Two Dimensional Numerical Simulation of the Marseille University Free-Piston Shock-Tunnel TCM2," *Proceedings of the 18th International Symposium on Shock Wave*, Vol. 1, Springer-Verlag, 1991, pp. 583-590.

[6]Zeitoun, D., "Chemical and Vibrational Nonequilibrium Flowfields," *Journal of Computational Methods in Applied Mechanics and Engineering*, Vol. 90, 1991, pp. 687-692.

[7]Stupochenko, Y. V., Losev, S. A., and Osipov, A. I., "Relaxation in Shock Waves," *Relaxation Processes in Shock Waves*, Springer-Verlag, Berlin, 1967, pp. 259-322.

[8]Park, C., "On Convergence of Computation of Chemically Reacting Flows," AIAA Paper 85-0247, Jan. 1985.

[9]Marrone, P. V., and Treanor, C. E., "Chemical Relaxation with Preferential Dissociation from Excited Vibrational Levels," *Journal of Physics of Fluids*, Vol. 6, No. 9, 1963, pp. 1215-1221.

[10]MacCormack, R. W., "Current Status of Numerical Solutions of the Navier-Stokes Equations," AIAA Paper 85-0032, Jan. 1985.

[11]Nebbache, A., and Zeitoun, D., "Application of an Implicit Numerical Method to the Computations of Laminar and Turbulent Flows," *Numerical Method in Laminar and Turbulent Flow*, Vol. 6, Pt. 2, Pineridge, Swansea, UK, 1989, pp. 1399-1409.

[12]Desideri, A., and Perriaux, J., *Workshop on Hypersonic Flows for Reentry Problems*, Test Case 8.2, Vol. II, Springer-Verlag, Berlin, 1990, p. 31-34.

[13]Gnoffo, P., "Application of Program LAURA to Thermochemical Nonequilibrium Flow Through a Nozzle," *Workshop on Hypersonic Flows for Reentry Problems*, Vol. II, Springer-Verlag, Berlin, 1990, pp. 1145-1158.

[14]Wilke, C. R., "A Viscosity Equation for Gas Mixtures," *Journal of Chemical Physics*, Vol. 18, No. 4, 1950, pp. 517-519.

[15]White, F. A., *Viscous Fluid Flow*, McGraw-Hill, New York, 1974, pp. 28-36.

[16]Boccaccio, E., "Etude des Ecoulements Hypersoniques Dissipatifs en Desequilibre Thermochimique: Application aux Tuyeres," Ph.D. Dissertation, Dept. of Fluid Mechanics, Université de Provence, Marseille, France, Sept. 1992.

[17]Druguet, M. C., Zeitoun, D., and Brun, R., "Inviscid Hypersonic Nozzle Flows in Chemical and Vibrational Nonequilibrium State," *Computing Methods in Applied Sciences and Engineering*, edited by R. Glowinski, Nova Science Publishers, New York, 1992, pp. 729-738.

[18]MacCormack, R. W., and Candler, G. V., "The Solutions of the Navier-Stokes Equations Gauss-Seidel Line Relaxation," *Computers and Fluids*, Vol. 17, No. 1, 1989, pp. 135-150.